Statistical adaptivity in PIV interrogation for mean flow estimation

Raf Theunissen[1], Fulvio Scarano[2], Michel L.Riethmuller[1]

[1] von Karman Institute for Fluid Dynamics, Sint-Genesius Rode, Belgium, raf.theunissen@vki.ac.be (✉), riethmuller@vki.ac.be
[2] Aerospace Engineering, Delft University of Technology, Delft, The Netherlands, f.scarano@lr.tudelft.nl

Abstract This paper addresses the robustness of adapting interrogation parameters to instantaneous image and flow conditions. It is shown that when the interest lies in mean flow fields the imposed instantaneous adaptive criteria are not optimal. Instead a new routine is proposed where interrogation parameters i.e. window size and overlap factor, take into account ensemble statistics over an entire image set. Correlation windows are now sized and located based on the average seeding density and average flow field variance. Compared to the instantaneous approach this statistical adaptivity locates more adequately the correlation windows and further allows the implementation of non-isotropic windows (stretching and orientation) which further improves the attainable spatial resolution. By means of a recursive procedure the necessary number of correlation samples to satisfy a prescribed window overlap ratio can be limited. With respect to more classical metrologies the routine thus offers a combination of strong computational advantage with superior resolution while requiring no user dependency whatsoever. The principle of the procedure is explained and demonstrated through application to the experimental case of a shock-wave boundary layer interaction.

Nomenclature

θ	correlation window orientation (radians)	I	image intensity
λ	nearest neighbor sample spacing (pixels)	IA	instantaneous adaptivity
φ	sampling rate, (number of windows per pix.)	N	local number of correlation windows
μ	velocity mean	N_w	total number of correlation windows
σ	velocity standard deviation	s	shock-normal coordinate
σ_I	intensity standard deviation	SA	statistical adaptivity
δs	infinitesimally small area (pixels^2)	u_{eq}, u_τ	van Driest and wall friction velocity
(ξ,η)	coordinate system rotated over angle θ with respect to (x,y) system	u_{n1}, u_{n2}	shock-normal velocity respectively upstream and downstream of the shock
(x,y)	coodinate system aligned with camera reference system	u', v'	Fluctuating velocity components in horizontal and vertical direction respectively
(x_i,y_i)	pixel coordinates	U_∞, U_e	free stream velocity, velocity at boundary layer edge
|X|	absolute value of X	WOR	window overlap ratio
<X>	ensemble average value of variable X	W_S	square correlation window size (pixels)
det(A)	determinant of A	Λ	Hessian eigenvalue
Ecc	correlation window eccentricity	T_e, T_{aw}	Temperature at boundary layer edge, adiabatic wall temperature
h	grid spacing (pixels)		
H	Hessian matrix		

1. Introduction

The analysis of PIV recordings by cross-correlation technique is nowadays fairly well established. Interrogation windows are placed on a Cartesian grid with node spacing h while keeping the square window size 'W_S' uniform throughout the image, leading to a general window overlap ratio '$WOR=1-h/W_S$'. The conventional interrogation analysis is hence dictated by two main parameters i.e. the window overlap ratio and minimum global window size which determine the spatial resolution. The PIV Challenges held (Stanislas *et al*., 2005) further attested the implementation of iterative window deformation and multigrid approaches (Scarano and Riethmuller, 2000) to have become standard practice. Although the latter has advocated an improvement in spatial resolution and process robustness, restrictions on the minimum window size remain inherent to the correlation's statistical nature. To retrieve reliable displacement estimates from cross-correlation, a study using synthetic images demonstrated the need of at least 7 effective particle image

doublets per correlation window (Keane and Adrian, 1990). While a minimum window size is imposed to yield a reliable signal measurement, the applied window overlap ratio must ensure an adequate vector spacing to properly sample and represent the flow. The sample spacing has been shown to have a large impact among others on vorticity estimations (e.g. Fouras and Soria 1998).
Tracer spacing can be optimized by modifying the seeding amount in the experimental setup and the spatial range by proper image magnification (Adrian, 1991). The requirements on WOR and minimum window size on the other hand automatically set an isotropic vector spacing throughout the image, irrespective of spatially and temporally varying flow features and seeding conditions. However, the way flow-related information is carried does not necessarily comply with the imposed processing parameters when confronted to real applications. Especially in industrial environments the recordings are exposed to spatial and temporal variations in seeding density, additional spurious reflections and higher image noise levels due to limited optical access. As such, the displacement measurements from real images typically suffer from inferior reliability concomitant of either finite spatial resolution or vector outliers.
To overcome the bottleneck of globally applied interrogation parameters, Theunissen *et al.* (2007) proposed a methodology whereby correlation window size and location (and as a result also the sample spacing), were automatically adapted to instantaneous conditions captured by single snapshots. While interrogation windows remain uniform in shape and orientation, Scarano (2003) proposed the application of non-uniform Gaussian windowing functions to reduce the measurement error related to the flow field curvature while simultaneously increasing the spatial resolution. It is important to realize that while the question of interrogation accuracy is suitably answered by reducing the effects of velocity gradients through image deformation, the spatial response is related to flow curvature. The latter explains the substantiality of window non-isotropy. Eigenvalues of the Hessian tensor containing the second order derivatives are based on the velocity components and allow the elliptical weighting functions to be determined. In this work, the adaptive interrogation analysis has been extended to include orientation of the interrogation windows based on flow curvature estimates to further improve the spatial resolution and extend the conventional image interrogation's limits. Typically the orientation and stretching are based on the iteratively determined displacement field after validation of the returned vectors. However, this methodology is sensitive to the robustness of the instantaneous image interrogation analysis. The susceptibility to outliers cause the curvature estimates to divergence from the true values when basing the procedure on individual snapshots. In turn, these estimates yield improper window stretching and orientation leading to nefarious consequences when implemented within a recursive structure. Instead, as the interest often lies in mean flow statistics, a reformulation of the adaptivity and weighting criteria to ensemble average statistics is therefore in order. In the remainder of the paper, the authors will propose a possible extension of the adaptivity criteria to enhance the adopted methodology's robustness and speed up the calculations.
The availability of a large image data set allows minimization of the degrading influence of noise by taking into account its intrinsic stochastic nature (Westerweel, 2000). Compromising between a limited set of statistical results and increased reliability, Meinhart *et al.* (2000) introduced the concept of ensemble correlation now commonly applied in micro-PIV (Wereley *et al.*, 2002). By averaging the ensemble of correlation maps for a given sample location prior to its analysis, the dominant peak becomes more prominent while spurious noise peaks reduce in amplitude. The presented work here goes in line of ensemble correlation in that the statistical information contained within an image data set is iteratively used to adequately size and locate the interrogation windows. The interrogation procedure presented by Theunissen *et al.* (2007) is extended to include non-uniform sampling and filter shapes (i.e. correlation windows) conform to the ensemble averaged tracer concentration (signal adaptivity), spatial variance and curvature in the mean velocity field (flow adaptivity).
The objective is the improvement of robustness and spatial resolution of mean velocity measurements. Because computer generated images fail to embrace all recording conditions encountered in real-life experiments the viability of the proposed interrogation technique will be assessed by application to a challenging experimental flow; the shock-wave boundary layer interaction.

2. Underlying rationale

From a theoretical point of view, PIV constitutes in principle a spatially filtered solution of the Reynolds averaged Navier-Stokes equations which form an analytical basis for insight in reigning flow dynamics. In most cases the turbulent energy is generated from mean shear, as indicated by the Reynolds stress transport

equation (Durbin and Pettersson Reif, 2000). These gradients in mean velocity are furthermore responsible for the production of vorticity and are in direct relation with the flow length scales. In general, finer sampling resolution is therefore required near discontinuities or steep curves in *mean* velocity. Analogous to computational methods, locating the positions that have large magnitudes of variance from the smooth curve serves as a good heuristic that indicates the regions for refinement. Considering the case of a shock-wave boundary layer interaction, a sampling density as depicted in Fig. 1-a would therefore be ideal. The incoming and reflected shock are over-sampled as is part of the boundary layer region (indicated by red dashed line) closest to the wall. The expansion downstream of the reflected shock as well as the shock-boundary layer interaction region is more densely sampled compared to the flow areas of uniform displacement.

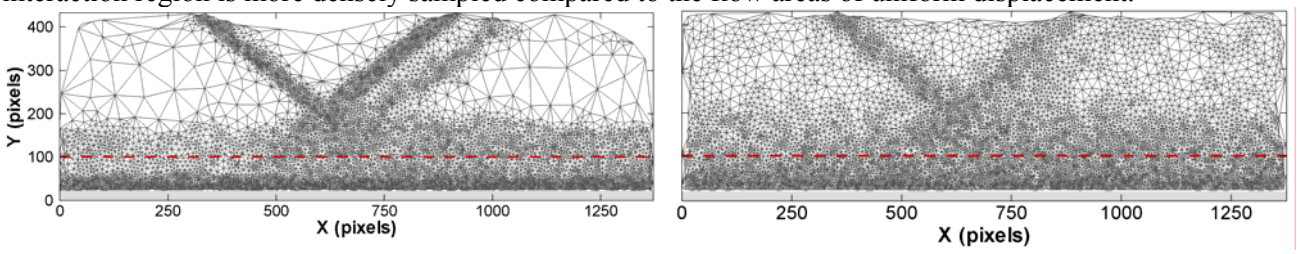

Fig. 1: Applied sampling locations (a) ideal situation (b) average over the instantaneous sampling locations.

To circumvent the ruling trade-off in requirements and the implicit fixed vector spacing, Theunissen *et al*. (2007) proposed an interrogation procedure which automatically adapts both correlation window size and location to locally instantaneous seeding conditions and flow structures i.e. velocity gradients. Plotting the *average* over 400 instantaneous sampling locations (Fig. 1-b) clearly pictures a distribution of correlation windows less ideal compared to that of Fig. 1. Though the boundary layer region is densely sampled, it is not optimal in that the regions of uniform flow are attributed quite an amount of correlation windows while the discontinuities are vaguely discernible. The latter is caused by the turbulent boundary layer and the interaction zone to be regions of highest velocity variance. Together with adaptive interface interrogation (Theunissen *et al.*, 2008) these areas attract accordingly the majority of the correlation windows leaving fewer present near the shocks. This does not imply a failure of the imposed adaptivity criteria but is an unhappy consequence of the reigning flow dynamics. Nevertheless, the average of instantaneous sample locations is still more convenient compared to a structured grid with uniform spacing.

The presence of shocks further requires, locally, a certain amount of anisotropy in the window shape and orientation. Scarano (2003) already demonstrated the benefits in resolution when the correlation windows are parallel to the shock and are reduced in shock-normal size. The idea of non-isotropic interrogation areas is further attractive in flow recordings with a large field of view containing poorly resolved flow features of interest. Adaptation of the interrogation window parameters, i.e. orientation and aspect ratio, to instantaneous flow curvature estimates prior to the correlation operation is however susceptible to outliers, which will deteriorate the quality and robustness of the final results with increasing iteration number. Besides, according to Fouras and Soria (1998) the transmission of random measurement error in the estimation of displacement derivatives is strongly linked to the sampling separation with high spatial resolution offering low attenuation. Especially in the refined regions the high sampling density will hinder a reliable determination of the Hessian matrix if based solely on instantaneous velocity data as a result of the noise sources. An example of the instantaneous eccentricity field for the horizontal velocity component for the shock-wave boundary layer interaction case is presented in Fig. 2-b. Small spatial variations in velocity cause non-zero eccentricity even in those regions absent of velocity gradients.

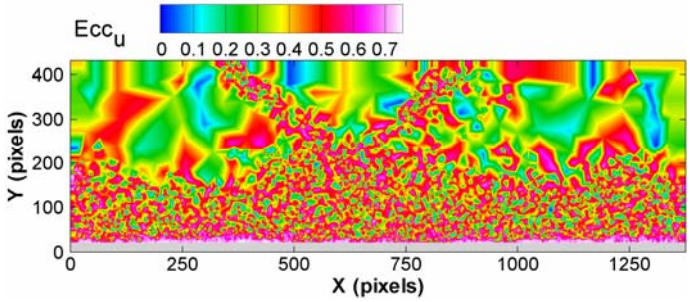

Fig. 2: Shock-wave boundary layer interaction: instantaneous eccentricity field for the horizontal velocity component.

Adapting the interrogation parameters to instantaneous conditions for each single snapshot is furthermore very time consuming considering the main interest in mean flow conditions. For each image doublet, the seeding concentration and particle motion must be iteratively determined and combined into a spatial distribution for window size, 'W_S', location, 'φ', eccentricity, 'Ecc' and orientation 'θ'. Only after the analyses of all images can the instantaneous flow fields and distributions be ensemble averaged to yield an average velocity field and sampling function (Fig. 1-b). Nevertheless, the implemented adaptivity remains computationally advantageous compared to conventional methodologies where correlation windows are placed on the nodes of a Cartesian grid; to reach a similar resolution both in terms of window size and vector spacing, a total of over 30000 windows are required whereas both Fig. 1 and Fig. 2 contain 10000 locations.
To conclude, an interrogation methodology is required with the aim of retrieving reliable mean flow estimates. The routine must be robust with respect to outliers in the estimation of window shape and orientation. Simultaneously, the spatial resolution both in terms of sample spacing and window size, must improve compared to conventional image analyses implementing structured sampling grids. Moreover, a global reduction in computational effort must be envisaged for the procedure to be attractive.

3. Proposed methodology

3.1 General concept

In the following a possible procedure is presented to overcome the interrogation parameter selection's sensitivity to vector outliers and improve the overall robustness in spatial distribution of the correlation windows. The general layout remains unchanged compared to instantaneous adaptivity (Fig. 3-a); tracer concentration (signal adaptivity) and spatial velocity variance (flow adaptation) are combined to yield spatial distributions which describe the properties of the correlation windows being size, location, shape and orientation. However, the input for the adaptivity criteria now involves ensemble averaged estimates for signal and flow adaptivity as schematically presented in Fig. 3-b. The statistical averaging operation will serve as a filter, reducing the influence of random fluctuations in the tracer density and velocity field, thereby enhancing the reliability and robustness of flow curvature estimates, predicted window sizes and window locations.

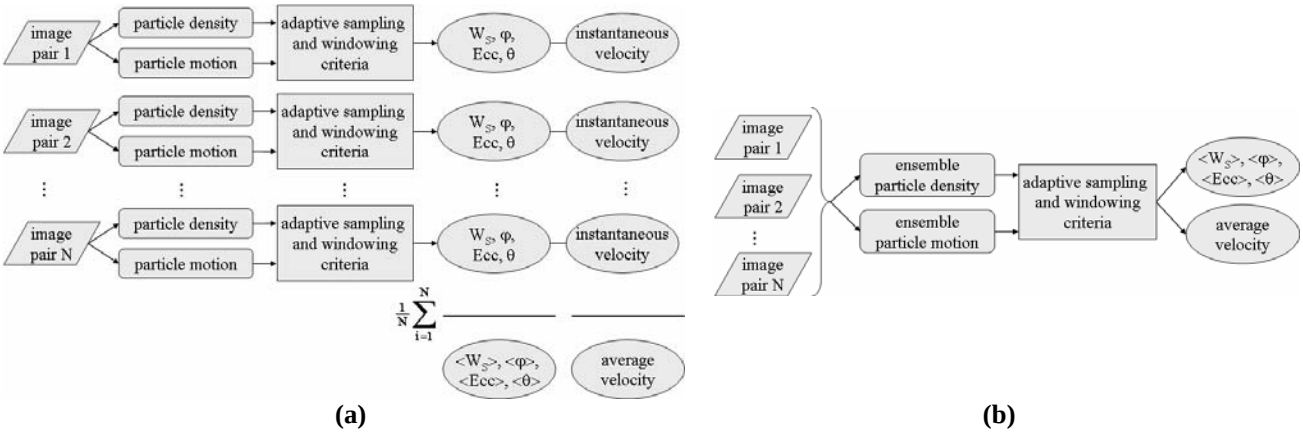

Fig. 3:. Flow diagram of interrogation adaptation to (a) instantaneous particle density and motion (b) ensemble particle density and motion.

Once the window characteristics have been determined, these remain unchanged throughout the analyses of the entire image set (Fig. 4). The distributions' rigidity poses however an important limit to the applicability of the proposed methodology. Because of the ensemble averaging, temporal fluctuations in flow velocity related to turbulence are irretrievable making the technique mainly apt for quasi-steady flows with low turbulence intensity. From that perspective, high signal-to-noise ratios, and thus high reliability in the measured mean displacement, can be obtained by averaging the correlation functions prior to locating the signal peak i.e. ensemble correlation according to Meinhart *et al.* (2000). It must be said though, that the shape of the correlation peak contains information concerning the statistical variation of the displacement (Kähler and Scholz 2006, Willert 2008).
Even in case of poor image quality ensemble correlation will remain robust and efficient in the extraction of the displacement estimates. On the other hand, the ensemble correlation map peaks at the *most probable* displacement. Only when the velocity probability distribution function is symmetric around the maximum will the location of the peak with highest amplitude correspond to the mean displacement. Still, to

accommodate a certain degree of freedom in the spread of the instantaneous correlation peaks around the origin, the snapshots could be re-analyzed individually, with a posterior averaging of the instantaneous velocity fields (Fig. 4).

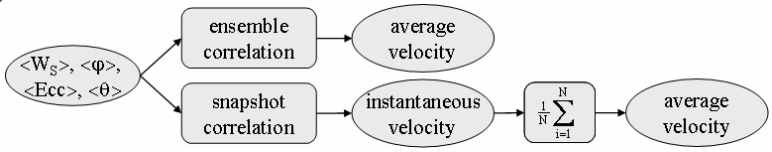

Fig. 4: Once the window characteristics have been determined they remain unchanged. An average velocity field can then be obtained either through ensemble correlation or correlating each snapshot.

3.2 Implementation

3.2.1 Signal adaptivity

Estimation of the ensemble particle density involves particle segmentation performed on the basis of an intensity threshold criterion. In line of the work of Stitou and Riethmuller (2001), the threshold is constructed from the mean intensity, '<I>', and RMS intensity, 'σ_I', calculated pixel wise;

$$I_{thresh} =< I > +1.5 \cdot \sigma_I \quad (1)$$

From the set of pixel intensities satisfying equation 1, only those constituting a spatially local maximum are considered as particles. The current selection criterion considers accuracy inferior to robustness in the estimation of signal quantity. The segmentation takes into account image noise to be typically associated with low pixel intensities compared to those belonging to particle images. Furthermore, the correlation operation is known to be more sensitive to higher image intensities (Young *et al.*, 2004), which is translated into the threshold requirement of the important signal to be sufficiently discernible from the surrounding intensities.

Imposing an adequate image density of 20 particle images automatically sets a lower limit on the local size of correlation window ensuring in average a sufficient number of tracer particles necessary for reliable correlation.

3.2.2 Flow adaptivity

To incorporate flow adaptivity, the routine starts by an iterative correlation of the images by means of fast Fourier transforms on a structured grid (Fig. 5). Window sizes are reduced from 81 pixels to 31 pixels in two refinement steps with iterative image distortion. This process is identical to the one described by Scarano and Riethmuller (2000). To further speed up the calculations windows overlap by 50%. A second pass refines the velocity estimates. This time the windows are distributed on an unstructured grid and have location and size prescribed by the outcome of the previous iteration. Note that the applied window characteristics are identical for each snapshot pair. The average velocity field obtained previously further serves as predictor in the deformation of the images.

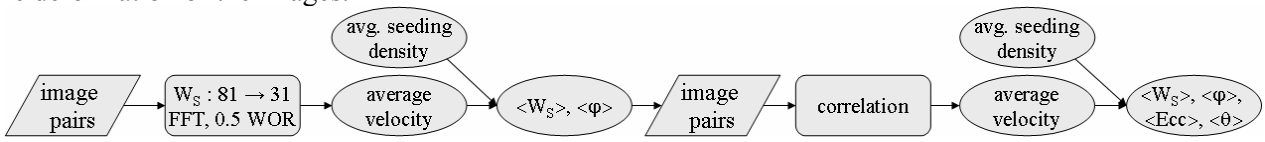

Fig. 5: Flow chart of the implemented methodology to retrieve a fast estimate of the correlation window characteristics.

3.2.3 Non-isotropic correlation windows

The non-isotropic window characterization is expressed through the eccentricity and orientation angle. At each window location, both parameters are derived for each displacement component from the relevant Hessian matrix, 'H', according to Scarano (2003). The Hessian matrix defined for the horizontal velocity component is recapitulated in (2) for clarity. After re-interpolating the average velocity field pixel-wise, second order derivatives are obtained by means of a parabolic Least-Square fit within a centered 11-by-11 kernel. Eccentricity and rotation angle are then expressed through the minimum and maximum eigenvalues, 'Λ', of the Hessian (equation 3). Because of the infliction point in the velocity profile across a shear layer or shock, the second derivatives tend to zero yielding zero eccentricity and rotation angle. To avoid this unphysical tendency, local eccentricity and angle are replaced by the maximum value within their immediate vicinity, followed by a sliding averaging operation.

$$\det\left(\mathrm{H}-\overline{\Lambda}\cdot\overline{\overline{1}}\right)=0 \quad \text{with} \quad \mathrm{H}=\begin{bmatrix}u_{xx} & u_{xy}\\ u_{xy} & u_{yy}\end{bmatrix},\ \overline{\overline{1}}=\begin{bmatrix}1 & 0\\ 0 & 1\end{bmatrix},\ \overline{\Lambda}=\begin{bmatrix}\Lambda_1\\ \Lambda_2\end{bmatrix} \text{ and } \begin{matrix}\Lambda_{min}=\min\left(|\Lambda_1|,|\Lambda_2|\right)\\ \Lambda_{max}=\max\left(|\Lambda_1|,|\Lambda_2|\right)\end{matrix} \tag{2}$$

$$\begin{cases}\theta=\operatorname{atan}\left(\frac{u_{xy}}{u_{xx}-\Lambda_{max}}\right)+\pi & \text{if } u_{xx}-\Lambda_{max}<0\\ \theta=\operatorname{atan}\left(\frac{u_{xy}}{u_{xx}-\Lambda_{max}}\right) & \text{else}\end{cases} \quad \text{and} \quad \mathrm{Ecc}=\tfrac{3}{4}\left(1-\frac{\Lambda_{min}}{\Lambda_{max}}\right)\cdot e^{-\frac{1}{\Lambda_{max}\cdot W_S\cdot 100}} \tag{3}$$

Window extensions along the major, 'ξ', and minor axis, 'η',are then given as respectively

$$W_{S,\xi}=W_S\cdot\frac{1}{\sqrt{1-\mathrm{Ecc}}} \quad \text{and} \quad W_{S,\eta}=W_S\cdot\sqrt{1-\mathrm{Ecc}} \quad \text{with} \quad W_S=\sqrt{W_{S,x}\cdot W_{S,y}} \tag{4}$$

Rather than applying intensity weighting functions the current method involves a reshaping and rotation of the interrogation areas. The consequently necessary intensity re-interpolation is performed by means of quintic B-splines (Unser *et al.*, 1993).

3.2.4 Number of correlation windows

When correlation windows are placed on the nodes of a Cartesian grid with spacing 'h', the mean overlap ratio can be directly expressed as '$1-h\cdot W_S^{-1}$'. However, application of a high uniform WOR throughout the image introduces a needless over-sampling of flow regions where larger scales are encountered. The current adaptive algorithm applies a varying window size and sampling rate taking into account the average flow scales and seeding density. In turn, this negates the need of uniform vector spacing and allows a drastic reduction in number of correlation windows and consequently computational effort. A procedure is proposed relating the adequate number of correlation windows to local sampling rate and window size while respecting an imposed mean window overlap ratio of 0.75.

The probability density function according to which the sampling locations are projected onto the spatial domain (Secord *et al.*, 2002) will be referred to as 'φ', with a given window size distribution 'W_S'. Both distributions are functions of the spatial coordinates. Ideally, the number of equidistant samples located within an infinitesimal small area 'δs', centered on pixel coordinates '(x_i,y_i)' can be approximated by '$N(x_i,y_i)=N_w\cdot\varphi(x_i,y_i)\cdot\delta s$', where '$N_w$' is the overall total number of windows. Even though 'φ' is not necessarily uniform, locally the distribution can be assumed to be Poissonian (Adrian, 1991). According to Stephens (1972), the distribution for the distance 'λ' to the nearest neighbor then equals

$$f(\lambda)=2\cdot\xi^2\cdot e^{-\xi^2} \quad \text{with} \quad \xi=\lambda/\lambda_m \quad \text{and} \quad \lambda_m=(\delta s/N)^{1/2} \tag{5}$$

The latter represents the most probable nearest neighbor distance and serves as an indicator of the local sample spacing. With the estimate of equidistant samples, the expression for the local window overlap ratio is given in equation (6) followed by the spatially averaged window overlap ratio, '<WOR>'.

$$\mathrm{WOR}(x_i,y_i)=1-\lambda_m(x_i,y_i)\left[W_S(x_i,y_i)\right]^{-1}=1-\left[\sqrt{N_w}\cdot\sqrt{\varphi(x_i,y_i)}\cdot W_S(x_i,y_i)\right]^{-1} \tag{6}$$

$$<\mathrm{WOR}>=1-N_T^{-1}\sum_i^{N_T}\left[\sqrt{N_w\cdot\varphi(x_i,y_i)}\cdot W_S(x_i,y_i)\right]^{-1} \tag{7}$$

On the account of the dependency on the a-priori unknown number and location of the windows, a recursive operation is needed, minimizing '<WOR>' with respect to 'N_w'.

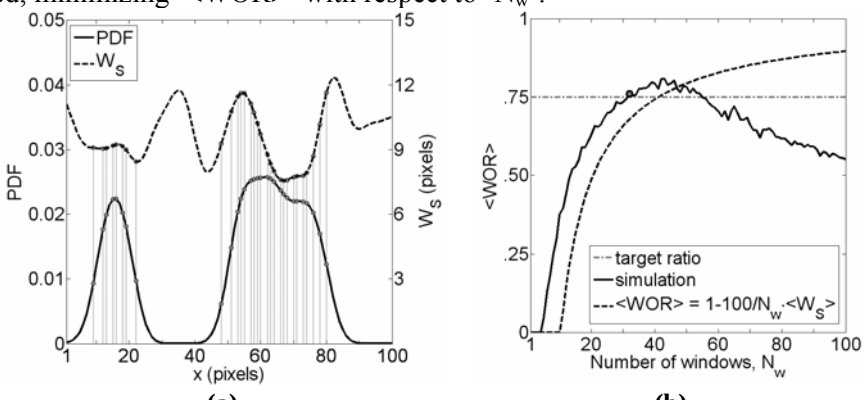

(a) **(b)**

Fig. 6: (a) Imposed sampling distribution function and window size (b) Evolution of the average WOR versus the number of windows. Sampling locations corresponding to an average WOR of 0.75 are indicated by gray lines in (a).

Without loss of generality a 1D example is considered in Fig. 6 within an interval of 100 pixels. Note however that for the 1D case the area 'δs' is also reduced in dimension and becomes a line segment yielding '$\lambda_m=(\delta s/N)$' which allows omitting the square root in equation (7). For each 'N_w', windows are spatially distributed according to the given PDF 'φ' and sized following the 'W_S' function (Fig. 6-a). As 'N_w' is gradually increased, the calculated '<WOR>' will surpass the imposed ratio indicating a sufficient number of samples (Fig. 6-b). The decrease in average overlap ratio is attributed to the saturation of the regions where '$\varphi>0$' with correlation windows when the minimum spacing between windows of 1 pixel is reached.

3.2.5 Statistical validation

Window characteristics and image deformation field are determined from the average velocity field. To minimize the nefarious influences of vector outliers in the determination of the mean flow field a robust statistical validation is a necessity. In the current work the routine is based on the validation procedure proposed by Heinz *et al*. (2002), assuming a normal probability density function for the local displacement. For each vector location, the Gaussian variance of the collection of displacements corresponding to that location is determined. Displacements exceeding three times the standard deviation in absolute value are excluded and the routine is repeated (Fig. 7) until convergence is reached.

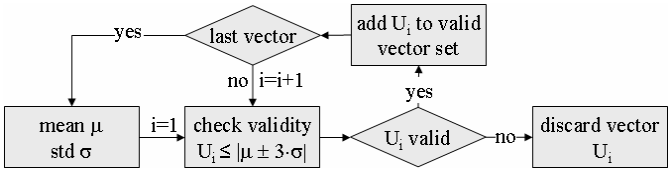

Fig. 7: Iterative statistical vector validation.

3.2.6 Image interrogation

As mentioned in paragraph 3.1, individual snapshots can be correlated once more utilizing the window characteristics determined from the ensemble average velocity field and tracer concentration. In the following more details are given concerning the implemented image interrogation (Fig. 8). When opted for ensemble correlation, the routine remains unchanged except for postponing the search for the correlation peak after averaging of the instantaneous correlation maps.
Prior to the correlation analysis, a background is subtracted from each of the recordings in an attempt to reduce the amount of image noise. The background noise estimate is based on the minimum pixel intensity throughout the image set (Wereley *et al.*, 2002).

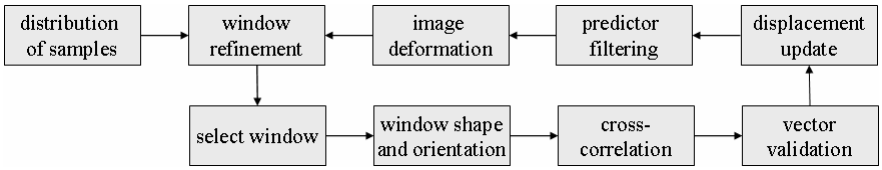

Fig. 8: Flow chart of the implemented image interrogation.

Following the spatial distribution, and sizing, correlation windows are stretched and rotated according to the pre-determined eccentricity and orientation distributions derived from the average velocity field. To allow for instantaneous deviations from the average velocity, the interrogation consists of two iterations with the first cycle applying twice the imposed window size.
A normalized cross-correlation coefficient is calculated either in a direct manner near interfaces or by means of Fourier transforms in the bulk of the flow (Theunissen *et al.*, 2008.). Sub-pixel accuracy in the displacement estimate is obtained by Gaussian fitting the highest peak in the final correlation function. To eliminate spurious vectors, validation involves a signal-to-noise threshold, a normalized median test (Westerweel and Scarano, 2005) and a convergence test of the corrective displacements. The latter states that with increasing iteration number the displacement peak should shift towards the origin of the correlation map after deforming the snapshots. Displacements flagged valid are re-interpolated using a 2nd order Least-Squares fit on the neighboring nodes, thereby stabilizing the predictor-corrector iterative interrogation (Schrijer and Scarano, 2006). To enlarge the measurable velocity gradient range, matching between regions which undergo transformation has to be improved. To do so, the images are deformed using B-splines (Unser

et al., 1993) based on a continuous first order approximation of the displacement field. The initial deformation field is given by the average displacements of the previous main iteration, but is updated by the instantaneous corrections for each individual image recording. This allows the measurement of instantaneous deviations from the average flow field. Though linear interpolation is in general less accurate compared to higher order interpolation schemes, it has the advantage of requiring less CPU. For this reason the predictor field for image distortion was constructed by means of a linear interpolation over all the pixels from the smoothened unstructured mesh of measurement points using the nearest neighbors (Sambridge *et al.*, 1995). Having reached the final image recording, the average flow field is retrieved from the statistical validation of the ensemble of instantaneous displacements.

4. Experimental application: Shock-wave boundary layer interaction

The performance of the proposed methodology is assessed through application on a set of experimental images of a shock-wave boundary layer interaction (Humble *et al.* 2006). The shock-wave boundary layer interaction has been chosen as it represents a challenging test case considering the presence of strong velocity gradients and both spatial and temporal intermittent seeding densities. Especially the formation of shocks, which requires a high spatial resolution, allows a thorough assessment of the proposed interrogation procedure. Experiments were conducted in a transonic-supersonic blow-down wind tunnel. A single-sided wedge with 10 degrees deflection angle was placed in the free stream at Mach 2.1 thus generating an oblique planar shock-wave. The latter impinges the fully developed turbulent boundary layer giving rise to a complex flow interaction. In total, 200 image snapshots were available in the analyses.
To provide a reference, the image set is additionally analyzed by means of a more conventional metrology. The conventional metrology involves iterative image deformation and reduction of correlation windows and is based on the procedure described by Scarano and Riethmuller (2000). In the current analyses two refinement steps were imposed leading to final window sizes of 21 pixels with 75% window overlap. Sampling locations correspond to the nodes of a Cartesian grid whereby window sizes and overlap factor are applied globally throughout the individual recordings and image set. The collection of velocity fields is post-processed afterwards to retrieve the mean flow field. A second iteration then repeats the image interrogation taking into account window eccentricity and orientation determined from the average velocity field.
In Fig. 9 the contours are shown of the horizontal velocity component following statistical adaptivity normalized with the free stream velocity. Incident shock and reflected shock are clearly distinguishable as well as the pocket of slow moving subsonic fluid below the interaction region with the turbulent boundary layer. A distinction is made in image interrogation between the wall region and free-stream (indicated by the dashed line). Near the interface, wall adaptivity will force more samples regardless of seeding density. The adaptive interface interrogation consists of window stretching parallel to the wall while gradually reducing the interrogation area. Further details concerning the improvement of the image analysis near a stationary interface can be found in Theunissen *et al.* (2008).

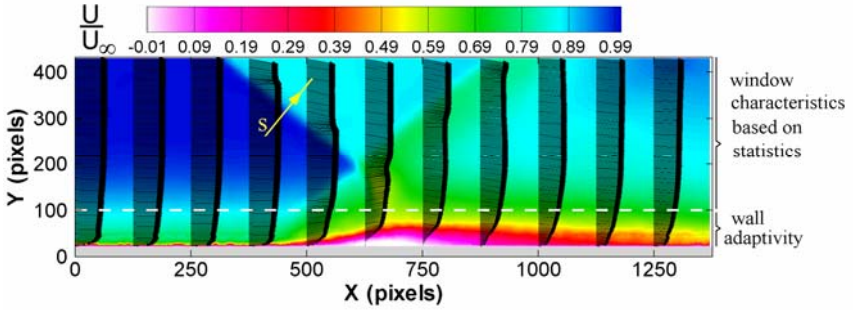

Fig. 9: Shock-wave boundary layer interaction: ensemble averaged contour field of the horizontal velocity component.

Figure 10 graphically displays the spatial distribution of correlation windows as determined by the outcome of the process sketched in Fig. 5. The different flow features can be easily inferred; the incoming and reflected shock, the expansion fan and the boundary layer region. Nine thousand samples are included leading to an average window overlap ratio of around 0.75 (Fig. 10-b). The strong reduction in sample spacing will omit any limitation in spatial resolution inherent to coarse vectors spacing. Of importance is the fact that to reach the same overlap coefficient and spatial resolution in the shocks when adopting a structured grid, around 40000 correlation windows are needed (Fig. 10-b). Clearly in case of the conventional,

structured approach the user would thus be confronted with a trade-off between computational efficiency and achievable spatial resolution. The proposed adaptivity therefore constitutes a considerable lowering of computational costs and accordingly computation time.

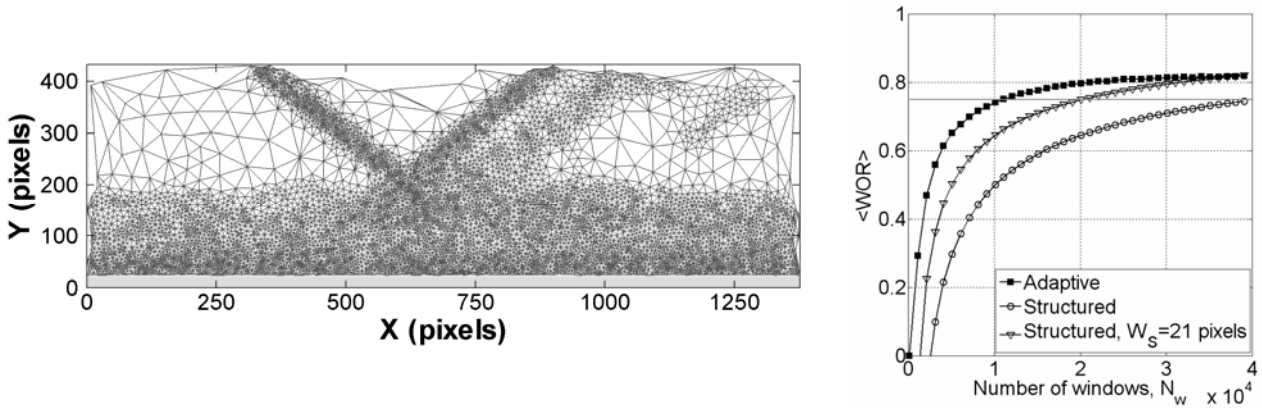

(a) **(b)**

Fig. 10: (a) Adaptive distribution of 9000 sampling locations. (b) Evolution of spatial averaged window overlap ratio with varying number of interrogation windows.

To further advocate the computational benefits, the partition in CPU time for a varying extent of image set is considered in Fig. 11. The total computational time is normalized by the time necessary to analyze a single snapshot with the instantaneous adaptivity approach. The latter serves as a reference unit. The first and second iterations refer to the analysis scheme presented in Fig. 5. Nine thousand correlation windows were involved. All image analyses methodologies obey a linear increase in CPU with number of images as indicated by the dashed line. Once the window characteristics have been determined, ensemble correlation (Fig. 4) yields the lowest computational effort (Fig. 11-b). The slightly higher CPU for the statistical adaptivity with snapshot correlation is attributed to the statistical vector validation routines. The conventional metrology leads to a doubling of the CPU when incorporating non-isotropic window characteristics (Fig. 11-c). Keeping in mind figure 10-b, the computational load will further increase when maintaining a spatial resolution equal to that achievable with the adaptive metrologies.

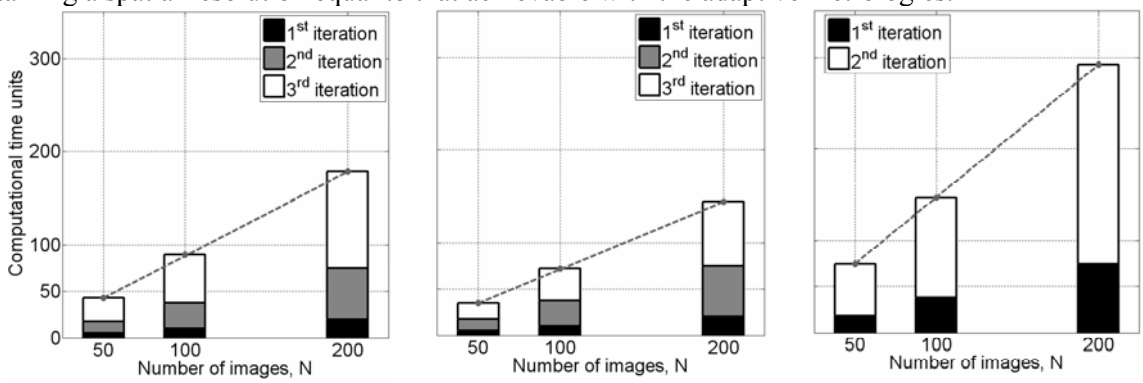

(a) **(b)** **(c)**

Fig. 11: Partition of computational effort. Statistical adaptivity with (a) snapshot correlation (b) ensemble correlation (c) conventional structured image analysis (final window size of 21 pixels with 75% mutual overlap).

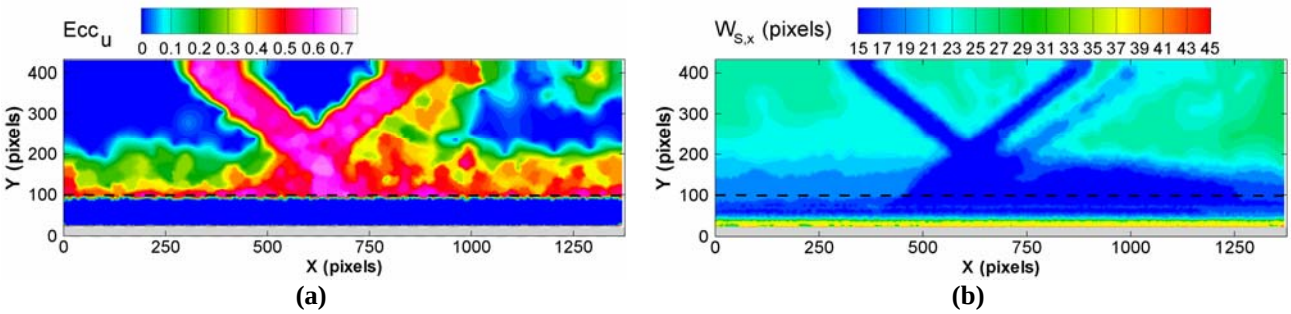

(a) **(b)**

Fig. 12: (a) Correlation window eccentricity and (b) square window-size according to the statistical adaptivity.

Besides a stretching of the correlation windows parallel to the shocks, windows are reduced in size to maximize the spatial resolution. Figure 12-a depicts the eccentricity of the windows for the horizontal velocity component. The eccentricity is clearly smeared across the shocks as a result of the filtering operations explained in paragraph 3.2.3. However, this also causes part of the boundary layer which is not submitted to wall-adaptivity to contain non-zero eccentricities. The square window sizes of 15 pixels in the vicinity of the shock combined with a typical maximum stretching of 0.5 yields a shock normal resolution of around 3 pixels. Near the wall a maximum stretching of 4 is imposed by wall adaptivity leading to wall-parallel window sizes of 37 pixels (Fig. 12-b) and 9 pixels in wall-normal direction. Within the conventional metrology square windows of 21 pixels^2 were applied. Combined with a global window overlap factor of 0.75, eccentricities of around 0.66 within the shock vicinity yield a resolution equal to that of the statistical adaptivity. As a result, the normalized profile of the velocity perpendicular to the shock taken along the abscissa 's' in Fig. 9, shows small discrepancies between the different assessed methodologies (Fig. 13-a). The considered methods are; statistical adaptivity followed by correlation of the snapshots ('SA-snapshot'), statistical adaptivity followed by ensemble correlation of the snapshots ('SA-ensemble'), interrogation with instantaneously determined adaptivity criteria ('IA') and the conventional metrology ('Conv.') after the 1st and 2nd iteration. The reason for the marginal improvements is that the shock-wave was already well resolved within the digital recording, causing the measured shock profile to be dominated by the particle response as shown in figure 13-a. The particle relaxation distance following the exponential fit depicted was estimated to be around 0.82mm, which is in reasonable agreement with the 0.76mm reported by Scarano and van Oudheusden (2003). It is worth noting that as such, the adaptive interrogation approaches are capable of returning results at least equal in quality to those obtained with the conventional metrology after a second iteration (!), but accompanied by a strong reduction in computational time and within an automated fashion absent of the need for user expertise.

Presented in Fig. 13-b are the velocity profiles within the undisturbed boundary layer as returned by the various interrogation approaches, expressed in inner-law variables 'u^+' and 'y^+'. Velocities are transformed into equivalent velocities following the concept of van Driest (8). For the current case the temperature at the edge of the boundary layer, 'T_e', reached 152K while the adiabatic wall temperature, 'T_{aw}', equaled 284K. The velocity at the boundary layer edge, 'U_e', was taken as 99% of the free stream velocity (525m/s). For further details the reader is referred to Humble *et al.* (2006). By zooming in on the boundary layer Humble *et al*. estimated the wall friction velocity, 'u_τ', with sufficient reliability to be 19.5 m/s.

$$u_{eq} = \frac{U_e}{a}\sin^{-1}\left(a\frac{u}{U_e}\right) = u_\tau\left(\frac{1}{\kappa}\log\left(y^+\right)+B\right) \quad \text{where} \quad a^2 = 1-\frac{T_e}{T_{aw}} \quad \text{with} \quad \kappa=0.41 \quad \text{and} \quad B=5.0 \tag{8}$$

None of the obtained velocity profiles correspond with the theoretical functions (Fig. 13-b). This does not come as a surprise as the current analyzed images were recorded at a larger field of view and suffer accordingly from degradation in digital resolution. This on the other hand allows a further assessment of the achievable spatial resolution. The conventional methodology performs worst but can slightly be improved by incorporating non-isotropy in window characteristics. Adaptation of the interrogation parameters to ensemble averaged flow and signal conditions is almost identical to instantaneous adaptation which is caused by the imposition of equal wall adaptivity criteria for both approaches. The importance of wall adaptivity is once more demonstrated as the achievable resolution is clearly supreme to the conventional metrology.

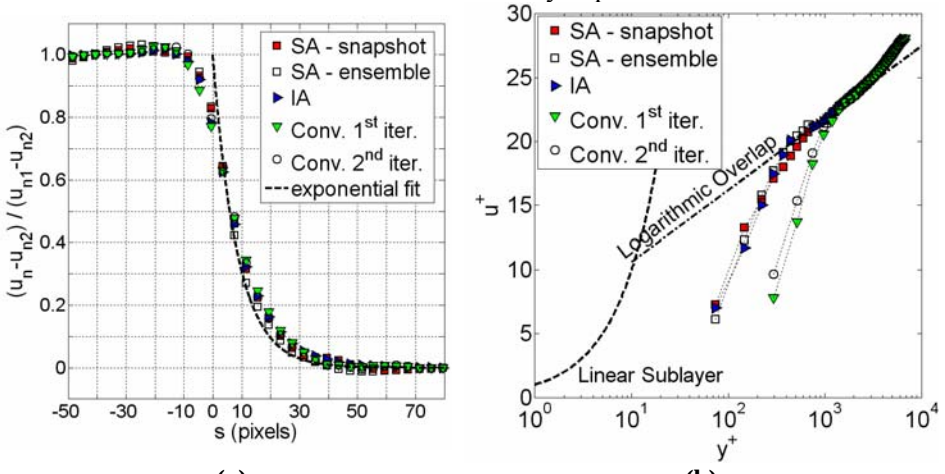

(a) **(b)**

Fig. 13: (a) Shock-normal velocity profile across the incident shock-wave (b) undisturbed boundary layer profile.

Finally, to demonstrate the computational efficiency of the proposed statistically adaptive interrogation method, shock-normal velocity profiles and boundary layer profiles are presented for a varying number of correlation windows 'N_w'. Two hundred image recordings were taken into account and analyzed with statistical adaptive interrogation followed by ensemble correlation (Fig. 4). The normalized CPU time is depicted in Fig. 14-a. A linear tendency can again be observed with increasing number of correlation windows. Imposing 1000 correlation windows clearly causes both the incident shock and boundary layer to be under-resolved (Fig. 14-b,-c). Convergence of the results for 'N_w' exceeding 5000 becomes evident as the remaining profiles superimpose nearly exactly. This result verifies the approach presented in paragraph 3.2.4 to be adequate in the selection of number of correlation windows and vindicates the computational efficiency of the proposed interrogation method.

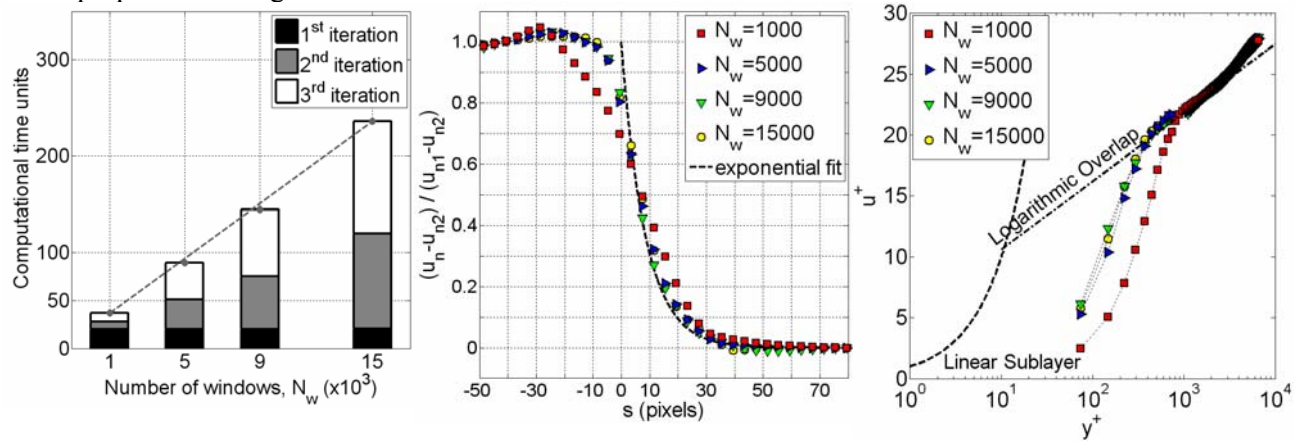

(a) **(b)** **(c)**

Fig. 14: (a) Partition of computational time for varying number of correlation windows (b) normalized, perpendicular velocity profile across the oblique shock-wave (b) undisturbed boundary layer profile in inner-law variables.

5. Conclusions

The application of PIV has become standard practice within a broad field of fluid dynamics. Commonly the image recordings are interrogated placing correlation windows on structured grids while setting window parameters, i.e. overlap and size, as global values. However, to account for spatial and temporal flow and seeding conditions, these window parameters can be set to adapt instantaneously. Under the assumption of quasi-steadiness in reigning flow, this instantaneous adaptivity can however be too computationally intense while the main interest lies in the mean flow field. Moreover, imposing non-isotropic window characteristics to account for curvatures within the flow (and thus improving spatial resolution) becomes unreliable when the necessary coefficients are based on instantaneous flow fields.

This paper sets out to remain in line with spatial variation in interrogation parameters by means of imposing adaptivity criteria, but simultaneously aim at retrieving reliable mean flow estimates. Furthermore, the sought for routine must be robust with respect to outliers in the estimation of window shape and orientation while enhancing computational efficiency and maintaining spatial resolution both in terms of sample spacing and window size. The authors propose an iterative routine which combines the robustness of conventional interrogation processes with the enhanced performances of adaptive interrogation. Rather than adapting to instantaneous conditions, window characteristics being shape, size, orientation and location are based on average flow field and average seeding concentration. The routine initializes by computing an estimate of the average velocity by means of a fast image analysis applying 32-by-32 pixels^2 correlation windows placed on a structured grid yielding 50% overlap. A second pass refines the window spatial distribution and sizes. The obtained mean flow field can then be utilized in the window characterization followed by either a final image interrogation pass involving either ensemble correlation or individual snapshot correlation. To accommodate a reduction in number of interrogation windows, a procedure is proposed which automatically computes the number of necessary windows obeying a window overlap ratio of 75%.

Application to the case of a shock-wave boundary layer interaction demonstrated a reduction in computational effort by at least a factor 2 while improving the spatial resolution compared to conventional interrogation routines. Moreover, the interrogation procedure was completely autonomous negating the need of user experience. With respect to instantaneous adaptation non-isotropic window characteristics were more reliable with a simultaneous reduction in computational load.

Acknowledgement

The PIV images of the shock-wave boundary layer interaction were kindly provided by Ray Humble from TUDelft Aerospace Engineering. The presented work is supported by the Instituut voor de aanmoediging van innovatie door Wetenschap & Technologie in Vlaanderen (IWT, SBO project nr. 040092).

References

Adrian R J, 1991, Particle-imaging techniques for experimental fluid mechanics, *Annual review of Fluid Mechanics*, 23, 261–304

Durbin P A and Pettersson Reif B A, 2001, Statistical theory and modeling for turbulent flows, John Wiley & Sons Ltd., 47-57

Fouras A and Soria J, 1998, Accuracy of out-of-plane vorticity measurements derived from in-plane velocity field data, *Experiments in Fluids*, 25, 409-430

Heinz O M, Ilyushin B B and Markovich D M, 2002, PIV-data validation algorithm based on statistical analysis for ensemble of turbulent velocity fields, *11th Int. Symp. Appl. laser techniques to fluid mechanics*, Lisbon, Portugal, 8-11 July

Humble R A, Scarano F and van Oudheusden B W, 2006, Experimental Study of an Incident Shock Wave/Turbulent Boundary Layer Interaction Using PIV, *36th AIAA Fluid Dynamics Conference and Exhibit*, San Francisco, California, 5-8 June

Kähler C and Scholz U, 2006, Transonic jet analysis using long-distance micro-PIV, *12th International symposium on flow visualization*, Göttingen, Germany, 10-14 September

Keane R D, Adrian R J, 1990, Optimization of particle image velocimeters. Part I: Double pulsed systems, *Measurement Science and Technology*, 1, 1202-1215

Meinhart C D, Wereley S T and Santiago J G, 2000, A PIV algorithm for estimating time-averaged velocity fields, *Journal of Fluids Engineering*, 122, 285-289

Sambridge M, Braun J and McQueen H, 1995, Geophysical parametrization and interpolation of irregular data using natural neighbours, *Geophysical Journal International*, 122, 837-857

Scarano F and Riethmuller M L, 2000, Advances in iterative multigrid PIV image processing, *Experiments in Fluids*, 29, S51–S60

Scarano F, 2003, Theory of non-isotropic spatial resolution in PIV, *Experiments in Fluids*, 35, 268–277

Scarano F and van Oudheusden B W, 2003, Planar velocity measurements of a two-dimensional compressible wake, *Experiments in Fluids*, 34, 430-441

Schrijer F F J and Scarano F, 2006, On the stabilization and spatial resolution of iterative PIV interrogation, *13th Int. Symp. Appl. laser techniques to fluid mechanics,* Lisbon, Portugal, June 26-29

Secord A, Heidrich W and Streit L, 2002, Fast primitive distribution for illustration, *In: 13th Eurographics Workshop on Rendering*, ed. P Debevec and S Gibson

Stanislas M, Okamoto K, Kähler C J and Westerweel J, 2005, Main results of the second international PIV challenge, *Experiments in Fluids*, Special Issue, DOI 10.1007/s00348-005-0951-2

Stephens J J, 1971, Distance distributions for randomly distributed data, *Monthly weather review*, 100, 60-61

Stitou A and Riethmuller M L, 2001, Extension of PIV to super resolution using PTV, *Measurement Science and Technology*, 12, 1398-1403

Theunissen R, Scarano F and Riethmuller M L, 2007, An adaptive sampling and windowing interrogation method in PIV, *Measurement Science and Technology*, 18, 275-287

Theunissen R, Scarano F and Riethmuller M L, 2008, On improvement of PIV image interrogation near stationary interfaces, *Experiments in Fluids*, DOI:10.1007/s00348-008-0481-9

Unser M, Aldroubi A and Eden M, 1993, B-spline signal processing: part II-efficient design and applications, *IEEE Transactions on Signal Processing*, 41-2, 834-848

Wereley S T, Gui L and Meinhart C D, 2002, Advanced algorithms for microscale particle image velocimetry, *AIAA*, 4-6, 1047-1055

Westerweel J and Scarano F, 2005, A universal detection criterion for the median test, *Experiments in Fluids,* 39, 1096-1100

Westerweel J, 2000, Theoretical analysis of the measurement precision in particle image velocimetry, *Experiments in Fluids*, 29, S3-S12

Willert C, 2008, Potential of ensemble-correlation techniques for adaptive PIV processing, *EWA Int. workshop on Advanced meas. tech. in aerodynamics*, Delft, The Netherlands, 31 March-1 April